Electrochimica Acta 55 (2010) 3528–3536

Contents lists available at ScienceDirect

Electrochimica Acta

journal homepage: www.elsevier.com/locate/electacta

Hydrogen spillover phenomenon: Enhanced reversible hydrogen adsorption/desorption at Ta_2O_5-coated Pt electrode in acidic media

Shunsuke Sata [a], Mohamed I. Awad [a,b], Mohamed S. El-Deab [a,b,1], Takeyoshi Okajima [a], Takeo Ohsaka [a,*,1]

[a] Department of Electronic Chemistry, Interdisciplinary Graduate School of Science and Engineering, Tokyo Institute of Technology, 4259-G1-5 Nagatsuta, Midori-ku, Yokohama 226-8502, Japan
[b] Department of Chemistry, Faculty of Science, Cairo University, Cairo, Egypt

ARTICLE INFO

Article history:
Received 29 September 2009
Received in revised form 19 January 2010
Accepted 20 January 2010
Available online 28 January 2010

Keywords:
Electrocatalysis
Hydrogen spillover
Stoichiometric oxides
Tantalum oxide
Hydrogen adsorption

ABSTRACT

The current study is concerned with the preparation and characterization of tantalum oxide-loaded Pt (TaO_x/Pt) electrodes for hydrogen spillover application. XPS, SEM, EDX and XRD techniques are used to characterize the TaO_x/Pt surfaces. TaO_x/Pt electrodes were prepared by galvanostatic electrodeposition of Ta on Pt from LiF–NaF (60:40 mol%) molten salts containing K_2TaF_7 (20 wt%) at 800 °C and then by annealing in air at various temperatures (200, 400 and 600 °C). The thus-fabricated TaO_x/Pt electrodes were compared with the non-annealed Ta/Pt and the unmodified Pt electrodes for the hydrogen adsorption/desorption (H_{ads}/H_{des}) reaction. The oxidation of Ta to the stoichiometric oxide (Ta_2O_5) increases with increasing the annealing temperature as revealed from XPS and X-ray diffraction (XRD) measurements. The higher the annealing temperature the larger is the enhancement in the H_{ads}/H_{des} reaction at TaO_x/Pt electrode. The extraordinary increase in the hydrogen adsorption/desorption at the electrode annealed at 600 °C is explained on the basis of a hydrogen spillover–reverse spillover mechanism. The hydrogen adsorption at the TaO_x/Pt electrode is a diffusion-controlled process.

1. Introduction

The term "spillover" refers to the surface mobility of active species formed (or sorbed) on one phase (called the initiator or the activator) to another phase called the acceptor, which does not generate these species under the given conditions [1,2]. It is a special case of surface migration of adsorbed species. Spillover phenomena have been observed for several small species such as hydrogen (and its isotopes) [3–17], oxygen [2,8,14–16,18,19], nitrogen [6,20] and carbon monoxide [21]. Hydrogen spillover is a promising phenomenon for hydrogen storage and is expected to open an avenue for realizing the fuel cell economy [22]. It usually occurs on supported metals with a well-known affinity to adsorb hydrogen dissociatively such as Ni, Ru, Rh, Pd and Pt [3–7]. Furthermore, hydrogen spillover has been observed at metal oxides and carbon-supported metal catalysts [17,23–35].

Recently, hydrogen spillover has been suggested as the primary reason for the improved CO-tolerance of Pt–Ru–Ni/C nanocomposite [36] as well as for the catalytic oxidation of CO at Pt/WO_3 and PtRu/WO_3 catalysts [37,38]. The importance of this process is justified for several vital industrial applications [39–50] e.g., hydrogenation of ethane [41] and in the development of hydrogen storage materials [40–42].

In the present study, a novel metal oxide modified Pt (TaO_x/Pt) electrode is prepared by electrodeposition of Ta from molten salts at 800 °C followed by annealing in air at various temperatures. The thus-prepared electrodes are characterized by electrochemical and surface analysis techniques. XPS results pointed to the formation of the stoichiometric Ta_2O_5 oxide, the amount of which is dependent on the annealing temperature. The electrocatalytic enhancement of the various TaO_x/Pt electrodes towards the hydrogen adsorption/desorption in acidic media is explained based on the so-called hydrogen spillover–reverse spillover mechanism. In our earlier communication [12], we have reported shortly on the observed phenomenon. In the current study the subject is treated in more detail in view of the phase, surface and electrochemical characterization of the TaO_x modified Pt electrodes. Furthermore, a plausible mechanistic approach of the phenomenon is given.

2. Experimental

2.1. Preparation of TaO_x/Pt electrodes

Electrodeposition of Ta was carried out in an electrochemical cell made of glassy carbon [12]. A smooth platinum plate of geometric area of 1.1 cm^2 was used as the working electrode. Spiral Pt wire and Ta wire served as the counter and quasi-reference elec-

* Corresponding author. Tel.: +81 45 924 5404; fax: +81 45 924 5489.
E-mail address: ohsaka@echem.titech.ac.jp (T. Ohsaka).
[1] ISE member.

0013-4686/$ – see front matter © 2010 Elsevier Ltd. All rights reserved.
doi:10.1016/j.electacta.2010.01.072

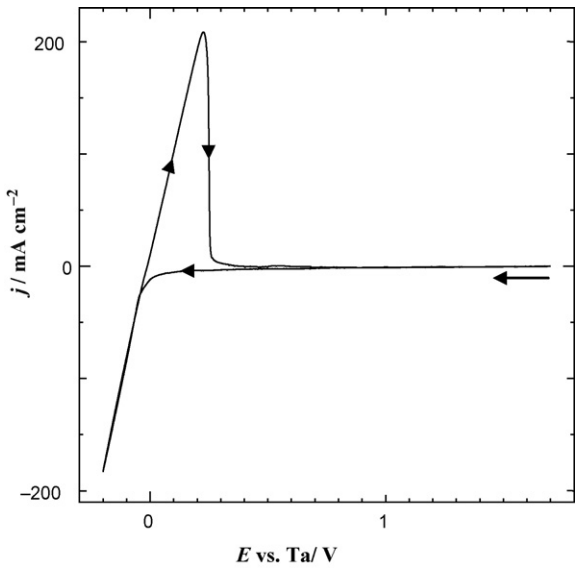

Fig. 1. Cyclic voltammogram obtained at Pt plate electrode in the potential range between −0.2 and 1.7 V in LiF–NaF molten salt containing K_2TaF_7 (20 mass%) at 800 °C. Potential scan rate: 100 mV s^{-1}.

trodes, respectively. The cell was filled with LiF–NaF (60:40 mol%) molten salts containing K_2TaF_7 (20 wt%) and then was placed in a chamber of IR electric furnace (RHL-P610C, ULVAC-RIKO, Inc.) and heated up to 800 °C under argon gas atmosphere. Electrodeposition of Ta onto Pt substrate was conducted in a controlled-current mode of typically −80 mA cm^{-2} for 10 min. Fig. 1 shows a typical cyclic voltammetric behavior of Pt plate in the above-mentioned molten salt. It shows that the deposition of Ta during the cathodic-going sweep takes place at potentials negative to −0.1 V according to:

$$TaF_7^{2-} + 5e^- \rightarrow Ta + 7F^- \quad (1)$$

An anodic dissolution peak of Ta is observed at ca. 0.23 V. The prepared Ta-modified Pt (Ta/Pt) electrodes were introduced into a muffle furnace (STR-12K, Isuzu Seisakusho Co., Ltd.) and annealed at three different temperatures, i.e., 200, 400 and 600 °C for 30 min in air atmosphere to prepare TaO_x/Pt electrode. Here it should be mentioned that after the Ta/Pt electrode was annealed at 600 °C the weakly attached surface TaO_x film (the thickness is roughly 50–100 μm) was peeled off leaving a thinner TaO_x film with the thickness of several μm. Thus, in the further surface and electrochemical characterization, the thus-obtained TaO_x/Pt electrodes were used. In the case of the annealing at 200 and 400 °C, such a peeling of the TaO_x film was not observed.

2.2. Electrochemical measurements

Electrochemical measurements were performed using an ALS/Chi 750B electrochemical analyzer. The working and the counter electrodes were separated by a porous glass. An Ag|AgCl|KCl(sat.) electrode was used as the reference electrode. A conventional three-electrode cell of around 20 ml was used for cyclic voltammetric measurements. All the electrochemical measurements were performed at room temperature (25 ± 1 °C) in aqueous solution of H_2SO_4 containing various amounts of Na_2SO_4. All current densities were calculated using the geometric surface area of the Pt electrode. Prior to Ta electrodeposition, Pt electrodes were electrochemically pretreated in N_2-saturated 0.05 M H_2SO_4 solution by repeating the potential scan in the range of −0.2 to 1.5 V vs. Ag/AgCl/KCl(sat.) at 100 mV s^{-1} for 10 min or until a reproducible CV of a clean polycrystalline Pt was obtained (see Fig. 6A, curve a).

2.3. Surface analysis

The SEM images of the different electrode surfaces were obtained using a scanning electron microscope (Keyence Company, Japan) at an acceleration voltage of 15 kV and a working distance of 7.5 mm. X-ray photoelectron spectroscopic (XPS) measurements of the various TaO_x/Pt electrodes were performed by ESCA3400 electron spectrometer (SHIMADZU) using an unmonochromatized X-ray source with Mg Kα (1253.6 eV) anode. X-ray diffraction (XRD) measurements were performed on a Philips PW 1700 powder X-ray diffractometer, using Cu $K_{\alpha 1}$ radiation (λ = 1.54056 Å) with a Ni filter working at 40 kV and 30 mA to identify the surface composition of the TaO_x/Pt electrodes.

3. Results and discussion

3.1. Surface and compositional characterization of the TaO_x/Pt electrodes

Fig. 2 displays typical SEM images of (a, a′) bare Pt, (b, b′) the as-electrodeposited Ta/Pt and (c, c′) TaO_x/Pt (annealed at 600 °C) electrodes at two different magnifications. Comparison of the apparent morphology of Ta/Pt (images b and b′) and TaO_x/Pt (images c and c′) indicates that the annealing process resulted in a significant lowering of the size of the granules with different microtopography.

The elemental analysis of the Ta/Pt electrode (by energy dispersive X-ray (EDX), shown in Fig. 3) (spectrum a) confirms the successful deposition of Ta on the surface of Pt electrode with the absence of any Pt signals. Whereas after annealing the Ta/Pt at 600 °C and peeling the surface TaO_x film (as mentioned in Section 2), the peaks of Pt and Ta are observed (spectrum b) indicating that the annealing process caused the partial exposure of the underlying Pt (possibly through the generation of cracks within the TaO_x layer as a result of the differences in the crystallographic structures of Ta and TaO_x (cf. Fig. 5)).

Furthermore, the chemical composition of the TaO_x/Pt electrodes has been probed using XPS. In Fig. 4 are shown the spectra of the 4f levels of Ta in (a) Ta/Pt and (b–d) TaO_x/Pt electrodes annealed at (b) 200, (c) 400 and (d) 600 °C. Each XPS spectrum is deconvoluted using the "Asymmetric Gaussian–Lorentzian Formula". Each deconvoluted spectrum shows several peaks for elemental Ta, partially oxidized tantalum (TaO_x, $x < 2.5$) and fully oxidized tantalum, i.e., the stoichiometric oxide (Ta_2O_5). At Ta/Pt (spectrum a) the Ta $4f_{7/2}$ and $4f_{5/2}$ binding energies for elemental Ta are shown at 21.6 and 23.5 eV, respectively, in agreement with the literature values for bulk tantalum [51]. The two peaks at 22.3 and 24.2 eV are indexed to tantalum suboxides (TaO_x, $x < 2.5$) [52,53]. The small shoulders at 26.5 and 28.5 eV correspond to Ta_2O_5 [54]. Inspection of spectra (b–d) reflects that the intensities of the peaks at 21.6 and 23.5 eV (corresponding to elemental Ta) are successively decreased with increasing the annealing temperature with a concurrent development of the two peaks at 26.5 and 28.5 eV (corresponding to Ta_2O_5). This indicates that the extent of oxidation of Ta into the stoichiometric oxide increases with the annealing temperature.

Fig. 5 presents XRD profiles of (a) Ta/Pt and TaO_x/Pt annealed at (b) 200, (c) 400 and (d) 600 °C. The XRD pattern shown in spectrum a displays three sharp peaks at 2θ of 37°, 54° and 69° corresponding to Ta (1 1 0), (2 0 0) and (2 1 1) facets, respectively [55]. Several interesting points can be extracted from this figure:

(i) Annealing the Ta/Pt electrode at 200 °C (spectrum b) caused insignificant change of the crystal structure compared with

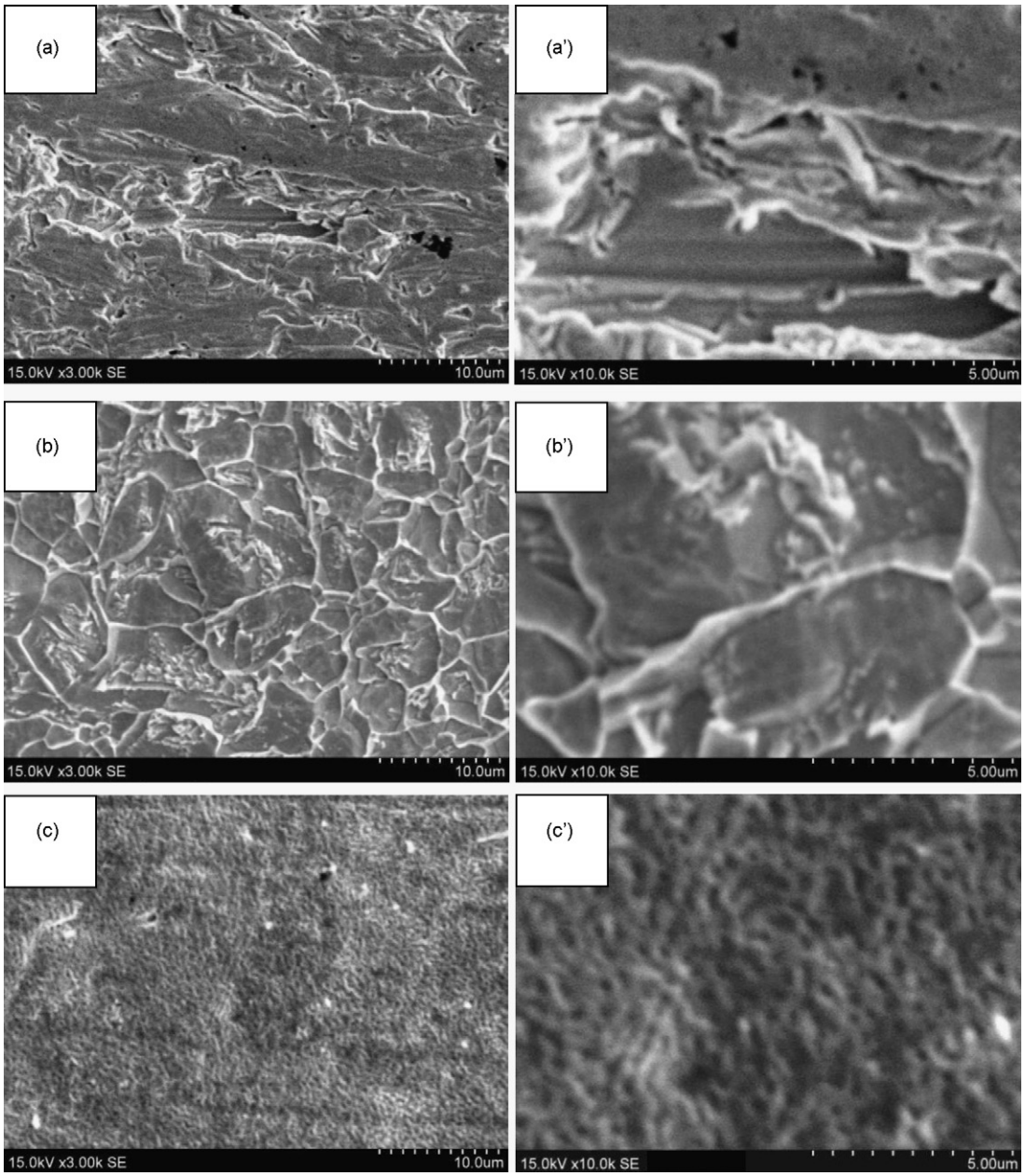

Fig. 2. SEM images of (a, a′) bare Pt, (b, b′) the as-electrodeposited Ta/Pt and (c, c′) TaO_x/Pt (annealed at 600 °C) electrodes at two different magnifications of (a, b, c) 3000× and (a′, b′, c′) 10,000×.

the non-annealed Ta/Pt (spectrum a) probably due to the low extent of oxidation at this temperature.

(ii) The increase of the annealing temperature to 400 and 600 °C (spectra c and d, respectively) results in the observation of several new peaks at 2θ of 23°, 28°, 37°, 50° and 56° which are indexed to Ta_2O_5 [56]. The higher the annealing temperature the larger is the intensity of these peaks, being consistent with the XPS observations (Fig. 4a–d).

(iii) The observation of diffraction peaks of Pt (spectrum d) for the sample annealed at 600 °C provides an evidence for the partial exposure of the underlying Pt substrate (in agreement with the results shown by EDX (Fig. 3)).

Based on the XPS and XRD data, it became evident that the stoichiometric oxide of Ta (Ta_2O_5) is the predominant chemical composition of the TaO_x/Pt annealed at 600 °C.

3.2. Electrochemical characterization of the enhanced hydrogen adsorption/desorption

3.2.1. Effect of annealing temperature

Fig. 6 shows cyclic voltammograms (CVs) obtained at (a) bare Pt, (b) Ta/Pt and (c) TaO_x/Pt electrodes in Ar-saturated 0.05 M H_2SO_4 solution. The TaO_x/Pt electrodes were annealed at (A) 200, (B) 400 and (C) 600 °C for 30 min. Two criteria can be employed to estimate the real surface area of bare Pt electrode, namely by estimating the amount of the charge consumed during either the reduction of Pt-oxide monolayer (at 0.45 V, curves labeled a) [57,58] using a reported value of 420 μC cm^{-2} or the (H_{ads}/H_{des}) reaction in the potential region 0.1 to −0.2 V using a reported value of 210 μC cm^{-2} [59]. The real surface area of the bare Pt electrode estimated by the two criteria is consistently the same. From CVs in Fig. 6, the amounts ($Q_{H_{des}}$) of charge consumed in the desorption process of hydrogen atoms at the Pt, Ta/Pt and Ta_2O_5 (or TaO_x)/Pt electrodes were esti-

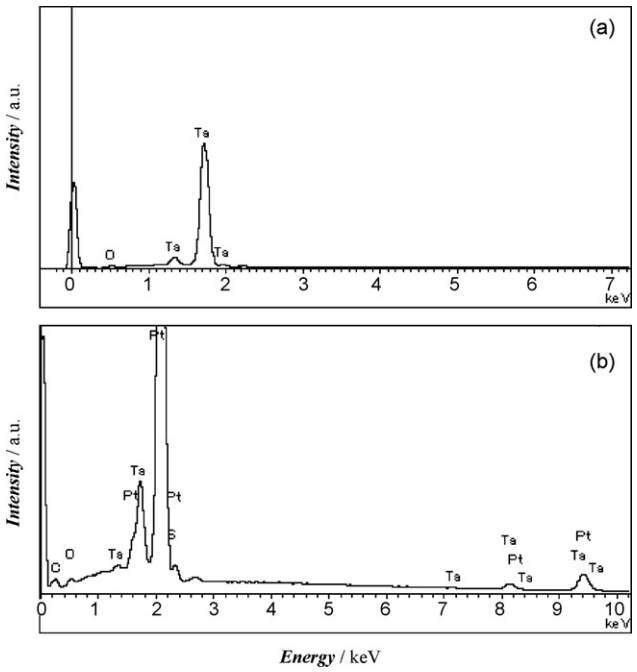

Fig. 3. EDX spectra of the surfaces of (a) Ta/Pt and (b) TaO_x/Pt electrodes. TaO_x/Pt electrode is annealed at 600 °C.

Table 1
The amount of charge consumed in the desorption process of hydrogen atoms ($Q_{H_{des}}$) at Pt, Ta/Pt and TaO_x/Pt electrodes measured in Ar-saturated 0.05 M H_2SO_4.

$Q_{H_{des}}$(Pt)[a] (μC cm^{-2})	$Q_{H_{des}}$(Ta/Pt)[a] (μC cm^{-2})	$Q_{H_{des}}$(TaO_x/Pt)[a,b] (μC cm^{-2})
480	4	7.7×10^3 (600 °C)
477	18	0.9×10^2 (400 °C)
483	72	1.0×10^2 (200 °C)

[a] $Q_{H_{des}}$(Pt), $Q_{H_{des}}$(Ta/Pt) and $Q_{H_{des}}$(TaO_x/Pt) show the amount of charge consumed in the desorption process of hydrogen atoms at Pt, Ta/Pt and TaO_x/Pt electrodes, respectively.
[b] Annealing temperatures are shown in parentheses.

mated and the results are given in Table 1. The estimated values of $Q_{H_{des}}$ of the unmodified Pt substrate (first column) are essentially the same (480 ± 3 μC cm^{-2}), while the $Q_{H_{des}}$ (Ta/Pt) values of the Ta/Pt electrodes (second column) are significantly smaller than those obtained at the unmodified Pt (albeit with large margin of variation). This possibly reflects the difficulty in controlling the surface coverage of Ta electrodeposited on the Pt substrate in the present electrolysis system even though the same experimental conditions are used (i.e., in LiF–NaF molten salt containing K_2TaF_7 at 800 °C). However, the major point to be stressed here is that an order of magnitude increase in $Q_{H_{des}}$ is observed upon the annealing of the Ta/Pt electrode at 600 °C (third column).

(i) In Fig. 6A: The electrochemical active area of bare Pt electrode is larger than that of either Ta/Pt electrode (curve b) or TaO_x/Pt

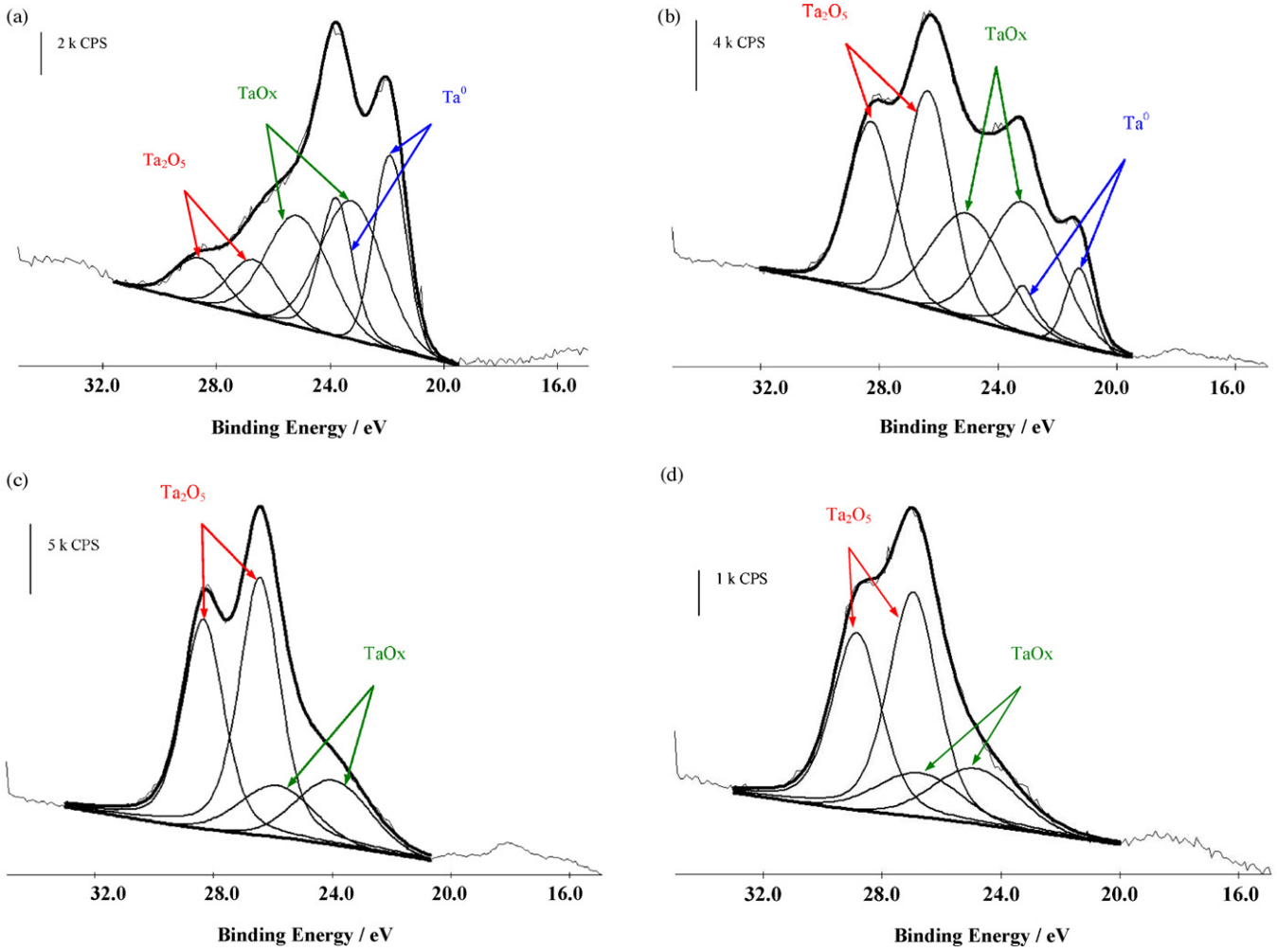

Fig. 4. Deconvoluted XPS spectra for Ta 4f of (a) as-electrodeposited Ta/Pt electrode and TaO_x/Pt electrodes calcinated at (b) 200, (c) 400 and (d) 600 °C.

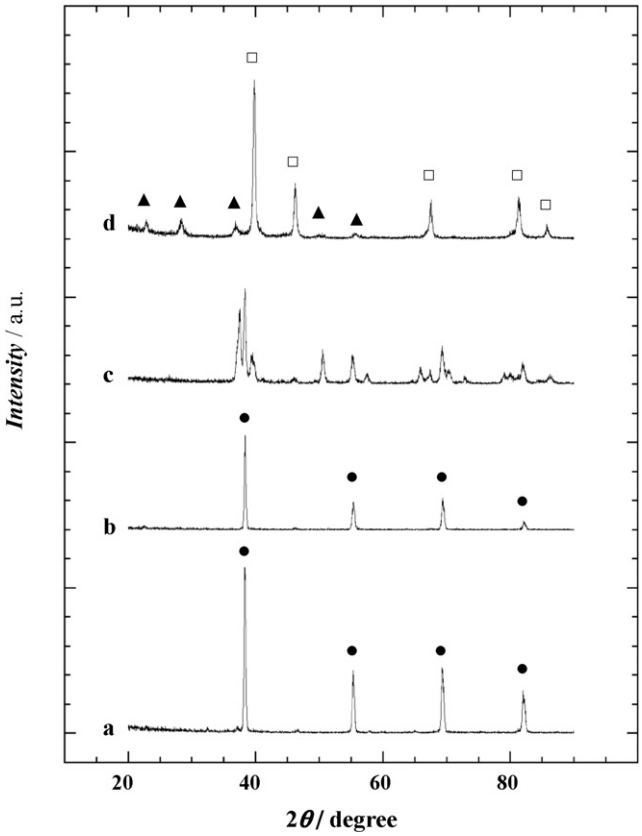

Fig. 5. XRD patterns of the surface of (a) Ta/Pt electrode and (b–d) TaO_x/Pt electrodes annealed at (b) 200, (c) 400 and (d) 600 °C. The peaks indicated by ●, ▲, and □ are assigned to Ta, Ta_2O_5 and Pt, respectively.

electrode annealed at 200 °C (curve c). The decrease of the exposed area of Pt in the Ta/Pt electrode (curve b) is due to the partial covering of the Pt substrate by the deposited tantalum as revealed from the EDX results. Comparison of curves b and c reveals a little enhancement in the hydrogen adsorption-desorption current (although the two electrodes have more or less the same Pt exposed area).

(ii) Similar results are also observed at TaO_x/Pt electrode annealed at 400 °C (see Fig. 6B).

(iii) The increase in the annealing temperature up to 600 °C (curve c in Fig. 6C) does not significantly affect the Pt-oxide reduction peak compared to that annealed at 400 °C (curve c in Fig. 6B). Interestingly, 81-fold increase of the amount of charge consumed during the H_{ads}/H_{des} is noticed at the former electrode (annealed at 600 °C). The enhancement in the H_{ads}/H_{des} process cannot be ascribed to the exposed Pt area but to a synergistic enhancement of TaO_x. That is frequently called a hydrogen spillover phenomenon. Hydrogen spillover can be assessed by calculating the hydrogen to metal ratio [36,60]. A ratio higher than unity is certainly due to hydrogen spillover whereas in the case of metals capable of forming hydrides, hydrogen spillover can be probed if the hydrogen to metal ratio exceeds the stoichiometric ratio of the hydride. Inspection of Fig. 6C curves a and c reveals that the H-spillover process at the Ta_2O_5/Pt electrode (curve c) starts at almost the same potential of the generation of the H_{ads} species at the unmodified Pt electrode (curve a). This implies that all the types of the generated H_{ads} (UPD and OPD) are being involved in the spillover process. Moreover, the $H_{ads/des}$ process at the unmodified Pt electrode shows a well-defined reversible behavior (two reversible peak couples). Whereas, at the Ta_2O_5/Pt electrode only one couple is observed (presumably due to the involvement of all the types of the generated H_{ads} in the spillover process).

It is noteworthy to mention here that the present system (i.e., Ta_2O_5/Pt electrode) shows a highly enhanced reversible behavior towards the hydrogen adsorption–desorption process. The enhancement factor (β) is given by:

$$\beta = \frac{(Q_{H_{ads}})_{mod}}{(Q_{H_{ads}})_{bare}} \quad (2)$$

where $(Q_{H_{ads}})_{bare}$ and $(Q_{H_{ads}})_{mod}$ are the charge consumed in the hydrogen adsorption at bare Pt and TaO_x/Pt electrodes, respectively. A value of β of ca. 16 was obtained at the Ta_2O_5/Pt electrode annealed at 600 °C. This indicates the superiority of the current system in the hydrogen adsorption process compared to other oxides [61]. For instance, enhancement factors of 5–10 were observed at Pt/Al_2O_3 and Pd/Al_2O_3 [61]. Moreover, the current system, advantageously, shows a reverse hydrogen spillover (i.e., migration of adsorbed hydrogen atoms from the support (TaO_x) to the catalyst (Pt)). This reversibility is verified by calculating the ratio of charge consumed during the hydrogen desorption ($Q_{H_{des}}$) to that consumed during the hydrogen adsorption ($Q_{H_{ads}}$). Fig. 7 shows the variation of $Q_{H_{des}}/Q_{H_{ads}}$ with potential scan rate. It shows that an almost constant ratio of unity is observed, indicating a high reversibility of the adsorption−desorption of hydrogen at the TaO_x/Pt.

3.2.2. Effect of pH

The effect of pH on the hydrogen adsorption–desorption has been studied extensively [62–65]. The hydrogen adsorption–desorption at a bare Pt electrode can be expressed as follows:

$$M + H^+ + e \rightleftarrows M\ldots H_{ads} \quad (3)$$

where M represents the surface atom of Pt electrode and H_{ads} refers to an adsorbed hydrogen atom. The inherent inclusion of protons in the above reaction indicates the pH dependence of the hydrogen adsorption/desorption. Fig. 8 compares the voltammetric behavior of (A) Pt electrode and (B) TaO_x/Pt electrode annealed at 600 °C in aqueous solutions containing x mM H_2SO_4 + (500 − x) mM Na_2SO_4 (x = 1, 5 and 50). Two pairs of well-defined redox couples characterize the hydrogen adsorption/desorption patterns at bare Pt electrode while at TaO_x/Pt electrode only one couple is observed. The voltammograms obtained at the bare Pt electrode are essentially the same in their shape except for their shift to the positive direction of potential with decreasing pH (Nernstian behavior). On the other hand, the hydrogen adsorption/desorption current at TaO_x/Pt electrode is remarkably increased with decreasing pH. In the case of TaO_x/Pt electrode the hydrogen spillover may continuously generate vacant active sites at the underlying Pt substrate for extra hydrogen adsorption and thus the current density increases with increasing the hydrogen ion concentration, although the reduction current of the Pt-oxide monolayer is kept constant actually.

For further electrochemical characterization of the observed cyclic voltammetric behaviors at the two electrodes, the potential scan rate dependence of the voltammetric behavior was measured at the two electrodes and the results are shown in Figs. 9 and 10. At the bare Pt electrode (Fig. 9), the ratio of the consecutive two anodic peaks to their counter cathodic peaks is almost unity (Fig. 7) with a peak potential separation close to zero indicating a high reversibility of the H_{ads}/H_{des} process at the unmodified Pt electrode. On the other hand, at the TaO_x/Pt electrode one couple of redox peaks is observed (Fig. 10A) (presumably due to the involvement of all the types of the generated H_{ads} (UPD and OPD) in the spillover process).

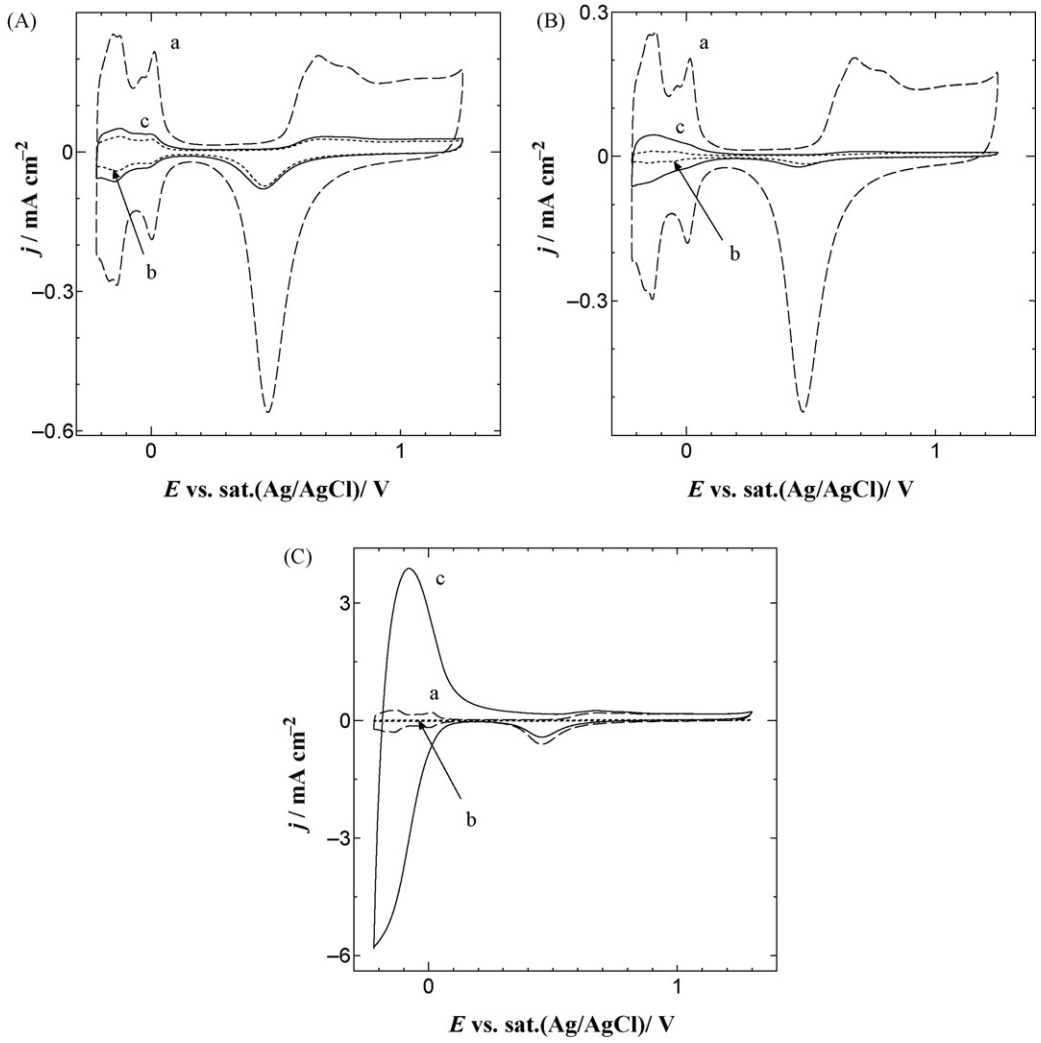

Fig. 6. CVs obtained at (a) bare Pt, (b) Ta/Pt and (c) TaO_x/Pt electrodes in Ar-saturated 0.05 M H_2SO_4 solution. The TaO_x/Pt electrodes were calcinated at (A) 200, (B) 400 and (C) 600 °C for 30 min.

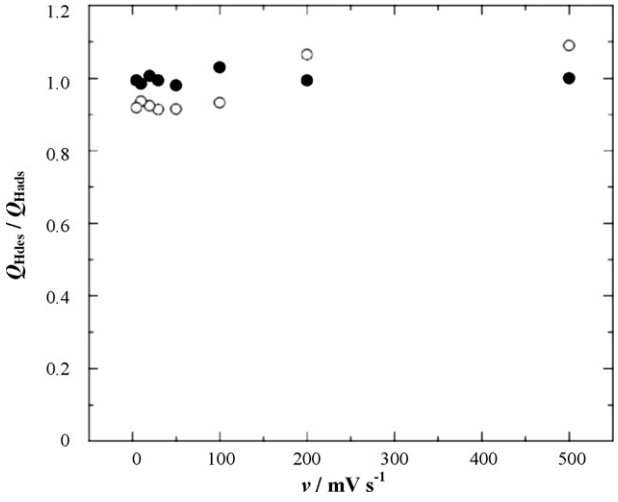

Fig. 7. Variation of $Q_{H_{des}}/Q_{H_{ads}}$ with potential scan rate for the hydrogen adsorption/desorption process at bare Pt (●) and TaO_x/Pt (annealed at 600 °C) (○) electrodes measured in Ar-saturated 50 mM H_2SO_4 + 450 mM Na_2SO_4 solution.

Furthermore, the peak current is proportional to the square root of scan rate $v^{1/2}$ (Fig. 10B) as expected for a diffusion-controlled process [66]. The increase of the anodic–cathodic peak potential separation of the H-spillover process with potential scan rate renders the reaction incompletely reversible. The increase in the peak separation could be attributed to the uncompensated solution resistance.

3.3. Mechanistic approach to the spillover phenomenon

Hydrogen evolution reaction (HER) at Pt electrode proceeds via several elementary steps including the generation of hydrogen atoms, which are adsorbed at different facets of the Pt electrode surface. In acidic media this reaction proceeds according to Eq. (3). The amount of charge consumed during the formation of H_{ads} is governed by the extent of the exposed real surface area of Pt substrate with a ratio of 210 μC cm^{-2} [59]. The observation of excessive charge greater than this ratio (although the exposed area of Pt is decreased with TaO_x coverage) refers to a spillover phenomenon.

The presence of metal oxides (e.g., TiO_2 [67–69], WO_3 [28,29,70–72], Al_2O_3 [13,73] or ZrO_2 [74,75]) in direct contact to the underlying Pt substrate (i.e., in the vicinity of the electrogenerated hydrogen atoms) is shown to promote another (electro-) chemical reaction that consumes the nascent generated $H_{(ads)}$, leading to an enhancement of the rate of Reaction (3). This process is well known

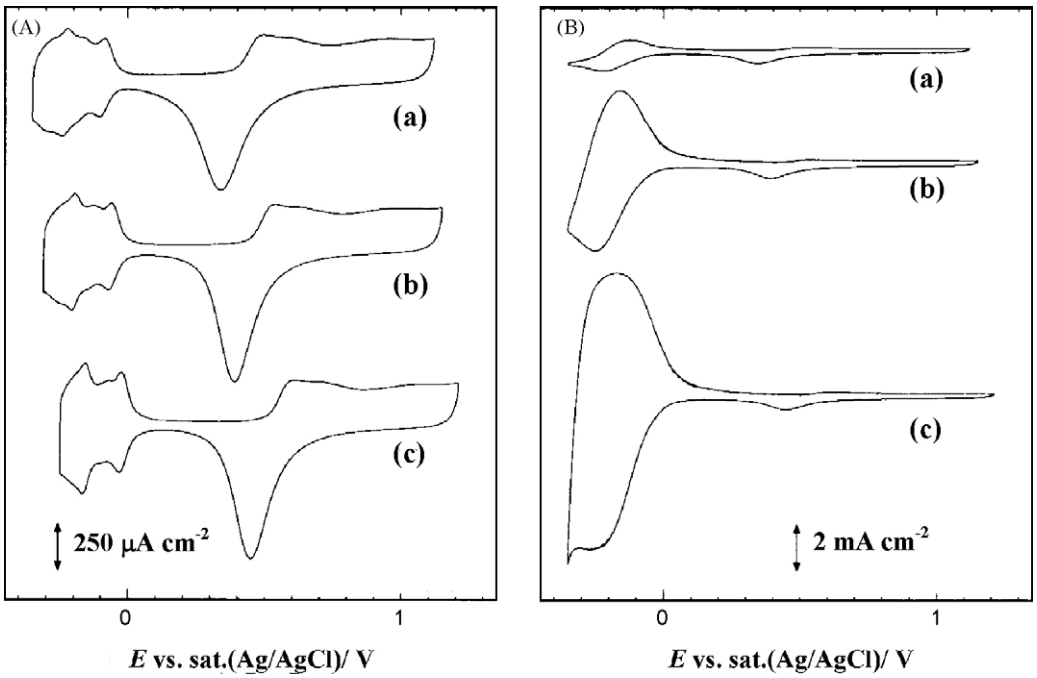

Fig. 8. CVs obtained at (A) Pt electrode and (B) TaO_x/Pt electrode annealed at 600°C in aqueous solutions of (a) 1 mM H_2SO_4 + 499 mM Na_2SO_4, (b) 5 mM H_2SO_4 + 495 mM Na_2SO_4 and (c) 50 mM H_2SO_4 + 450 mM Na_2SO_4. Potential scan rate: 100 mV s^{-1}.

as a spillover phenomenon. The current system (Ta_2O_5-coated Pt substrate) represents a typical example of this phenomenon. The adsorbed hydrogen atoms on some sites on the underlying Pt substrate migrate to the TaO_x, which acts as an acceptor for hydrogen adsorption leading to the availability of the Pt active sites for further adsorption of hydrogen to proceed. This resulted in the observed remarkable increase in the hydrogen adsorption at the TaO_x/Pt electrode annealed at 600 °C. This phenomenon has not been observed at the TaO_x/Pt electrodes annealed at lower temperatures, indicating the necessity of the Ta_2O_5 phase for a successful observation of the spillover phenomenon. The existence of Ta oxide in a stoichiometric structure (i.e., Ta_2O_5) is considered as the primary factor for the spillover phenomena, in which the electrogenerated $H_{(ads)}$ species are consumed via a series of reactions represented by:

$$O^{2-} + 2H_{(spill)} \rightarrow H_2O + V_O{}^{2-} \quad (4a)$$

where O^{2-}, $H_{(spill)}$ and $V_O{}^{2-}$ refer, respectively, to an oxide in Ta_2O_5 lattice, hydrogen atom generated at Pt and migrated to Ta_2O_5 lattice via spillover process and an oxygen vacancy which results from the removal of an oxide ion O^{2-} from a surface point in the lattice (i.e., generation of a defect site at the surface of the crystal lattice of the stoichiometric Ta_2O_5). As more oxygen vacancies are generated, the oxide deviates from its stoichiometry. The extent of this deviation can be expressed as δ in the formula $Ta_2O_{5-\delta}$. Thus, the above reaction can also be expressed as:

$$Ta_2O_5 + 2\delta H_{(spill)} \rightarrow \delta H_2O_{(ads)} + Ta_2O_{5-\delta} (\text{during the cathodic scan}) \quad (4b)$$

The continuous feed of H atoms from the underlying Pt substrate promotes Reaction (4) (a and b) in such a way that the number of oxygen vacancies ($V_O{}^{2-}$) increases at the surface of the Ta_2O_5 crystals and hence leads to the observed high Faradaic current during the cathodic scan due to the increase in the number of defects within the surface of the Ta_2O_5 lattice. This process is known as an autocatalytic mechanism, which is frequently used to explain the kinetics of the surface reactions [76]. As more oxygen vacancies are generated, the remaining Ta_2O_5 deviates from stoichiometry and hence the electronic conductivity (σ) of Ta_2O_5 increases accordingly. The extent of this deviation can be expressed as δ in the formula $Ta_2O_{5-\delta}$. σ is related to the concentration of the oxygen vacancies (n) by [76]:

$$\sigma = 2en\mu \quad (5)$$

where e is the electronic charge and μ is the mobility of the oxygen vacancies. As Reaction (4) proceeds n increases and hence σ does also increase. This is very much noticed during the cathodic potential scan in the potential region from 0 to −0.2 V (see Fig. 6C, curve c). It is noteworthy to mention here that Reaction (4) is effectively

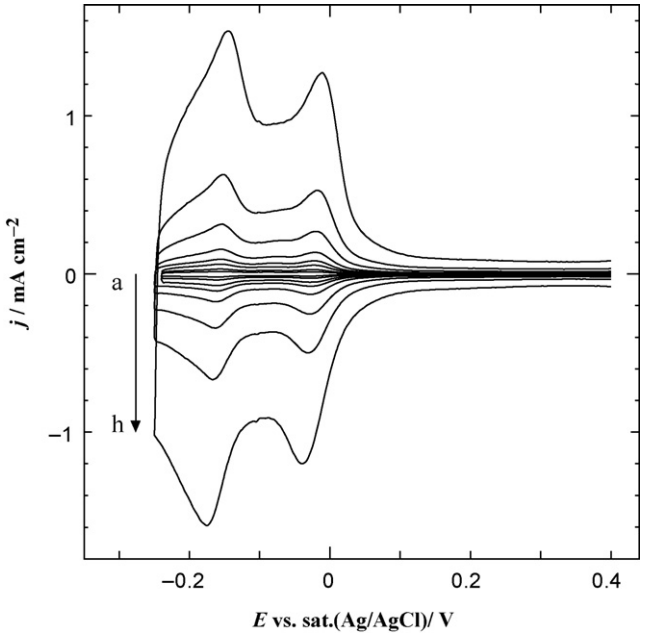

Fig. 9. CVs obtained at the bare Pt electrode in Ar-saturated 50 mM H_2SO_4 + 450 mM Na_2SO_4 solution. Potential scan rates: (a) 5, (b) 10, (c) 20, (d) 30, (e) 50, (f) 100, (g) 200 and (h) 500 mV s^{-1}.

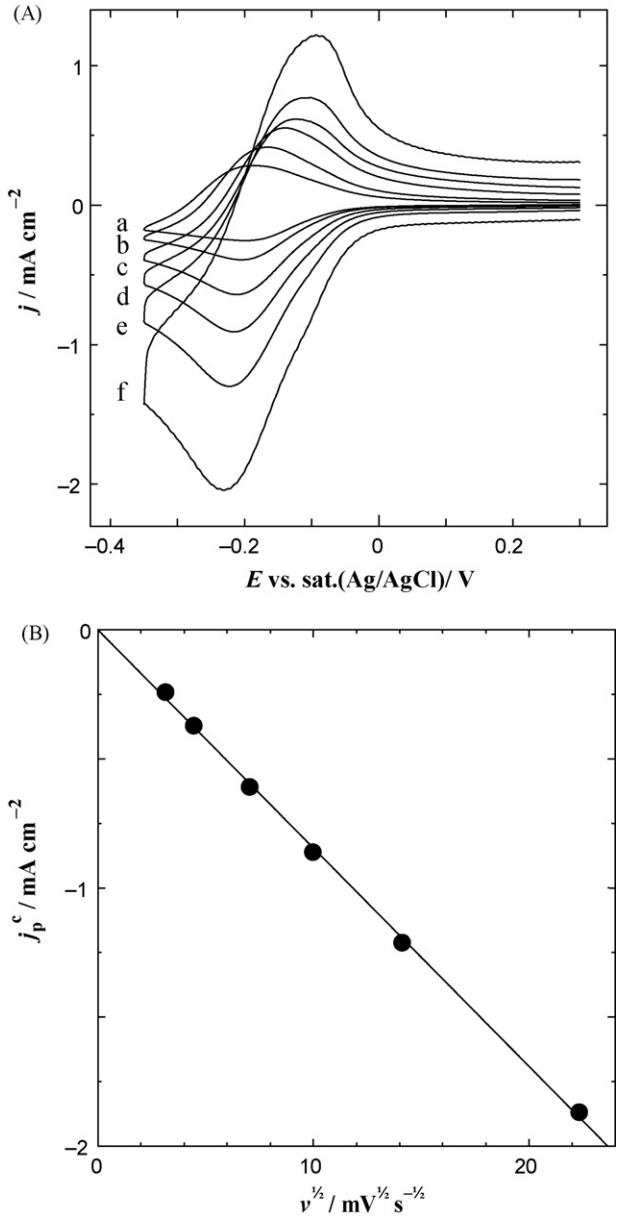

Fig. 10. (A) CVs and (B) j_p^c vs. v plots obtained at the Ta_2O_5/Pt electrode in Ar-saturated 50 mM H_2SO_4 + 450 mM Na_2SO_4 solution. Potential scan rates: (a) 10, (b) 20, (c) 50, (d) 100, (e) 200 and (f) 500 mV s^{-1}.

a surface diffusion-controlled reaction, which proceeds till the formation of a skin layer of the non-stoichiometric oxide is obtained. Thus, the extent of deviation from stoichiometry is governed by the amount of surface oxide ions in the Ta_2O_5. That is, the reaction is supposed to be terminated as a result of the diffusion limitation. In other words, the increase of the oxygen vacancies at the surface of Ta_2O_5 leads to a downward diffusion of the V_O^{2-} towards the bulk of the Ta_2O_5 crystal with a concurrent upward diffusion of oxide ions from the bulk towards the surface of the Ta_2O_5 crystal. This diffusion is thought to add another barrier to the overall reaction and is shown to be very slow at the ambient temperature, thus leading to the termination of the observed enhancement.

Whereas, during the anodic potential scan, an oxidation process takes place for the atomic hydrogen at the Pt substrate:

$$H_{(ads)} \rightarrow H^+ + e- \quad (6)$$

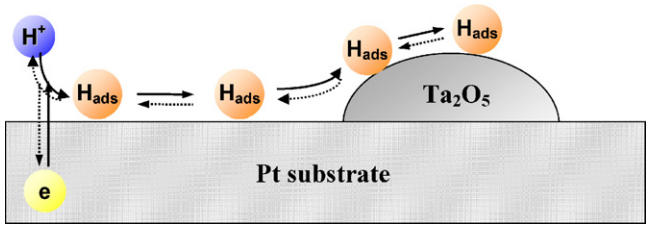

Scheme 1. A schematic illustration of hydrogen spillover–reverse spillover phenomenon over the Ta_2O_5/Pt electrode in acidic aqueous media. The arrows ⟶ and ⟵ show the reduction and oxidation processes, respectively.

And the reverse of Reaction (4b) takes place during the anodic potential scan, i.e.:

$$\delta H_2O_{(ads)} + Ta_2O_{5-\delta} \rightarrow Ta_2O_5 + 2\delta H_{(spill)} (\text{during the anodic scan}) \quad (7)$$

This reaction indicates the regeneration of the stoichiometric Ta_2O_5 as a result of the inclusion of oxide ions into the surface skin layer of the non-stoichiometric oxide. Furthermore, this reaction feeds the generated H atoms to the Pt surface (reverse-spillover), which are subsequently oxidized as described in Reaction (6). The feasibility of Reactions (3) and (6) are verified by the observed enhancement of the reaction current in the hydrogen adsorption/desorption region. Scheme 1 is an illustration of the hydrogen spillover–reverse spillover process at the Ta_2O_5 modified Pt electrode. It shows the electrogeneration of adsorbed hydrogen atoms (H_{ads}) at bare Pt spots (during the cathodic potential scan) which react momentarily with a surface lattice oxide of the adjacent Ta_2O_5, leading to the generation of oxygen vacancies at the surface skin layer and free Pt active sites. On the contrary, during the anodic potential scan, the release of hydrogen atoms takes place at the expense of the oxygen vacancies, i.e., the regeneration of the stoichiometric Ta_2O_5 occurs exclusively. It should be noted here that Ta_2O_5 itself is electroinactive under the present experimental conditions.

4. Conclusions

The current study addresses the hydrogen spillover phenomenon at tantalum oxide modified Pt (TaO_x/Pt) electrodes. Ta film was electrodeposited onto Pt substrate (Ta/Pt) and was subsequently subjected to annealing at various temperatures. XRD along with XPS techniques confirmed the formation of the stoichiometric oxide (Ta_2O_5) atop the Pt substrate upon annealing of the Ta/Pt at 600 °C in air. The formation of Ta_2O_5 is considered as a key factor in the observation of the enhanced hydrogen adsorption/desorption processes at TaO_x/Pt electrodes in acidic aqueous media. This is explained by a hydrogen spillover–reverse spillover phenomenon.

Acknowledgements

This work was financially supported by Grant-in Aids for Scientific Research (A) (No. 19206079) from the Ministry of Education, Culture, Sports, Science and Technology (MEXT), Japan and also by New Energy and Industrial Technology Development Organization (NEDO), Japan.

References

[1] W.C. Conner (Ed.), Proceedings of the 1st Hit. Conference Spillover, Lvons, France, 1983, Volume of Discussion, University of Claude Bernard, Lyon-Villeurbanne, 1984, p. 71.
[2] W.C. Conner, J.L. Falcone, Chem. Rev. 95 (1995) 759.
[3] W.C. Conner, in: P. Paal, G. Menon (Eds.), Hydrogen Effects in Catalysis, Marcel Dekker, New York, 1988, p. 311.

[4] M. Boudart, Adv. Catal. 20 (1969) 153.
[5] P.A. Sermon, G.C. Bond, Catal. Rev. 8 (1973) 211.
[6] W.C. Conner, G.M. Pajonk, S.J. Teichner, Adv. Catal. 34 (1986) 1.
[7] D.A. Dowden, in: C. Kemball, D.A. Dowden (Eds.), Catalysis, vol. VIII, Spec. Period. Rep., The Chemical Society, London, 1980, p. 136.
[8] B. Delmon, Heterogeneous Chem. Rev. 1 (1994) 219.
[9] L.-T. Weng, B. Delmon, Appl. Catal. A 81 (1992) 141.
[10] Z. Paal, P.G. Menon (Eds.), Hydrogen Effects in Catalysis, Marcel Dekker, New York, 1988.
[11] G.M. Pajonk, Appl. Catal. A 202 (2000) 157.
[12] S. Sata, T. Okajima, F. Kitamura, K. Kaneda, T. Ohsaka, Chem. Lett. 36 (2007) 572.
[13] F. Roessner, U. Roland, J. Mol. Cat. A: Chem. 112 (1996) 401.
[14] J.M. Jaksic, C.M. Lacnjevac, N.V. Krstajic, M.M. Jaksic, Chem. Ind. Chem. Eng. Quart. 14 (2008) 119.
[15] J. Jiang, B. Yi, J. Electroanal. Chem. 577 (2005) 107.
[16] W.G. Bessler, J. Warnatz, D.G. Goodwin, Solid State Ionics 177 (2007) 3371.
[17] C.I. Contescu, C.M. Brown, Y. Liu, V.V. Bhat, N.C. Gallego, J. Phys. Chem. C 113 (2009) 5886.
[18] B. Luerßen, S. Günther, M. Kiskinova, J. Janek, R. Imbihl, Chem. Phys. Lett. 316 (2000) 331.
[19] H. Lin, J. Mol. Cat. A: Chem. 144 (1999) 189.
[20] Z. Knor, C. Edelmann, J. Rudny, J. Stachurski, Appl. Surf. Sci. 25 (1986) 107.
[21] B. Sen, J.L. Falconer, T.-F. Mao, M. Yu, R.L. Flesner, J. Catal. 126 (1990) 465.
[22] B. Chen, J.L. Falconer, J. Catal. 134 (1992) 737.
[23] K. Ebitani, J. Konishi, H. Hattori, J. Catal. 130 (1991) 257.
[24] K. Ebitani, J. Tsuji, H. Hattori, H. Kita, J. Catal. 135 (1992) 609.
[25] H. Hattori, Stud. Surf. Sci. Catal. 77 (1993) 69.
[26] V.S. Bagotzky, L.S. Kanevsky, V.S. Palanker, Electrochim. Acta 18 (1973) 473.
[27] S. Srinivas, P. Rao, J. Catal. 148 (1994) 470.
[28] G.C. Bond, T. Mallat, J. Chem. Soc., Faraday Trans. 77 (1981) 1743.
[29] M. Boudart, A.W. Aldag, M.A. Vannice, J. Catal. 18 (1970) 46.
[30] A.J. Robell, E.V. Ballon, M. Boudart, J. Phys. Chem. 66 (1964) 2748.
[31] J.F.C. Candau, W.C. Conner, J. Catal. 106 (1987) 378.
[32] R.R. Cavanagh, J.T. Yates Jr., J. Catal. 68 (1981) 22.
[33] J.L. Robbins, E.M. Soos, J. Phys. Chem. 93 (1989) 2885.
[34] J.A. Lachawiec Jr., Q. Gongshin, R.T. Yang, Langmuir 21 (2005) 11418.
[35] S.C. Tsang, C.D.A. Bulpitt, P.C.H. Mitchell, A.J. Ramirez-Cuesta, J. Phys. Chem. B 105 (2001) 5737.
[36] Y. Liang, H. Zhang, Z. Tian, X. Zhu, X. Wang, B. Yi, J. Phys. Chem. B 110 (2006) 7828.
[37] K.Y. Chen, P.K. Shen, A.C. Tseung, J. Electrochem. Soc. 142 (1995) L185.
[38] P.K. Shen, K.Y. Chen, A.C. Tseung, J. Electrochem. Soc. 142 (1995) L85.
[39] G.E.E. Garde, G.M. Pajonk, S.J. Teichner, J. Catal. 33 (1974) 145.
[40] G. Dutta, U.V. Waghmare, T. Baidya, M.S. Hegde, Chem. Mater. 19 (2007) 6430.
[41] P. Bera, A. Gayen, M.S. Hegde, N.P. Lalla, L. Spadaro, F. Frusteri, F. Arena, J. Phys. Chem. B 107 (2003) 6122.
[42] B. Hariprakash, P. Bera, S.K. Martha, S.A. Gaffoor, M.S. Hegde, A.K. Shulka, Electrochem. Solid-State Lett. 4 (2001) A23.
[43] J. Kondo, N. Akamatsu, K. Domen, T. Onishi, J. Electron. Spectrosc. Relat. Phenom. 54/55 (1990) 805.
[44] J. Kondo, H. Abe, Y. Sakata, K. Maruya, K. Domen, T. Onishi, J. Chem. Soc., Faraday Trans. 84 (1988) 511.
[45] J. Kondo, K. Domen, K. Maruya, T. Onishi, J. Chem. Soc., Faraday Trans. 86 (1990) 3665.
[46] K. Domen, J. Kondo, K. Maruya, T. Onishi, Catal. Lett. 12 (1992) 127.
[47] J. Kondo, K. Domen, K. Maurya, T. Onishi, J. Chem. Soc., Faraday Trans. 86 (1990) 3021.
[48] J. Kondo, K. Domen, K. Maruya, T. Onishi, J. Chem. Soc., Faraday Trans. 88 (1992) 2095.
[49] T. Onishi, K. Maruya, K. Domen, H. Abe, J. Kondo, Proc. 9th Int. Cong. Catal. (Canada) 2 (1988) 507.
[50] W.C. Conner, G.M. Pajonck, S.J. Teichner, Adv. Catal. 34 (1986) 1.
[51] J.C. Fuggle, N. Martensson, J. Electron Spectrosc. Relat. Phenom. 21 (1980) 275.
[52] M. Zhu, Z. Zhang, W. Miao, Appl. Phys. Lett. 89 (2006) 1.
[53] J.-Y. Zhang, I.W. Boyd, Appl. Surf. Sci. 168 (2000) 234.
[54] F.J. Himpsel, J.F. Morar, F.R. McFeely, R.A. Pollak, G. Hollinger, Phys. Rev. B 30 (1984) 7236.
[55] T. Hino, M. Nishida, T. Araki, Surf. Coat. Tech. 149 (2002) 1.
[56] L. Liu, H. Gong, Y. Wang, J. Wang, A.T.S. Wee, R. Liu, Mater. Sci. Eng. C 16 (2001) 85.
[57] A.N. Frumkin, in: P. Delahy (Ed.), Electrochem. Electrochem. Eng., vol. 3, Wiley-Interscience, New York, 1963, p. 287.
[58] H.F. Hunger, J. Electrochem. Soc. 115 (1968) 492.
[59] S. Trasatti, O.A. Petrii, Pure Appl. Chem. 63 (1991) 711.
[60] A.D. Lueking, R.T. Yang, Appl. Cat. A: Gen. 265 (2004) 259.
[61] N.M. Popova, D.V.Tr. Sokol'skii, Inst. Org. Khim. Electrokhim. Akad. Nauk. Kaz. SSR 1 (1972) 1.
[62] R.E. White (Ed.), Comprehensive Treatise of Electrochemistry, vol. 4, 1981, p. 41.
[63] N.S. Marinković, N.M. Marković, R.R. Adžić, J. Electroanal. Chem. 330 (1992) 433.
[64] B.E. Conway, L. Bai, J. Electroanal. Chem. 198 (1986) 149.
[65] Yi-Fu Yang, Guy Denuault, J. Electroanal. Chem. 418 (1996) 99.
[66] A.J. Bard, L.R. Faulkner, Electrochemical Methods, Fundamentals and Applications, 2nd ed., Wiley, New York, 2001.
[67] D.V. Malevich, V.B. Drozdovich, I.M. Zharskii, Russ. J. Electrochem. 32 (1996) 298.
[68] D.V. Malevich, V.B. Drozdovich, I.M. Zharskii, Stud. Surf. Sci. Catal. 112 (1997) 359.
[69] D.V. Malevich, A.F. Masez, V.G. Matys, I.M. Zharskii, Stud. Surf. Sci. Catal. 138 (2001) 101.
[70] S.T. Srinivas, P.K. Rao, J. Catal. 148 (1994) 470.
[71] W.J. Liu, B.L. Wu, C.S. Cha, J. Electroanal. Chem. 476 (1999) 101.
[72] H. Takagi, H. Hatori, Y. Yamada, Chem. Lett. 33 (2004) 1.
[73] J.L. Robbins, E. Marucchi-Soos, J. Phys. Chem. 93 (1989) 2885.
[74] T. Shishido, H. Hattori, Appl. Catal. A 146 (1996) 157.
[75] H. Hattori, T. Shishido, Catal. Surv. Jpn. 1 (1997) 205.
[76] M.H. Abd Elhamid, M.M. Khader, A.E. Mahgoub, B.E. El Anadouli, B.G. Ateya, J. Solid State Chem. 123 (1996) 249.